

Bachelor Thesis

**Exploring earthquakes through their audible sound:  
Listening to the sound of earthquake Doppler and  
anelastic attenuation phenomena**



Menexopoulos Dimitris

Supervised by  
Costas Papazachos

Aristotle University of Thessaloniki  
School of Geology - Department of Geophysics

July 2014

## **Acknowledgements**

I would deeply like to thank Prof. Costas Papazachos for his unique open-mindedness, excitement and support in supervising my work on this particular topic. Moreover, I owe special thanks to Prof. Anastasia Kiratzi for providing several of the seismic records used in this study and to PhD student Chrisa Ventouzi for her constant help on collecting the necessary data for the needs of this thesis.

## Contents

<b>I.</b>	<b>Introduction</b>	
1.1.	Subject analysis and motivation.....	4
1.2.	Brief history of auditory seismology.....	5
1.3.	Methodology in outline.....	7
1.4.	Introduction to the main phenomena studied.....	8
1.4.1.	Doppler effect.....	8
1.4.2.	Anelastic attenuation.....	9
<b>II.</b>	<b>Doppler effect</b>	
2.1.	The Doppler phenomenon and its relation to seismology.....	10
2.2.	Sound processing of Doppler data from the 7/9/1999 M=5.9 Athens earthquake.....	14
2.2.1.	General information about the seismic event.....	14
2.2.2.	Data extraction and conversions.....	15
2.2.3.	Data processing.....	17
<b>III.</b>	<b>Anelastic Attenuation</b>	
3.1.	Attenuation types of seismic energy.....	20
3.2.	Active tectonics and anelastic attenuation in the Aegean region.....	22
3.3.	Acoustic study of the intermediate depth 27/7/2006 M=3.3 Nisiros earthquake.....	24
3.3.1.	General information about the seismic event.....	24
3.3.2.	Data extraction and conversions.....	25
3.3.3.	Data processing.....	26
<b>IV.</b>	<b>Discussion.....</b>	<b>29</b>
<b>V.</b>	<b>Conclusions.....</b>	<b>31</b>
<b>VI.</b>	<b>References.....</b>	<b>33</b>
<b>VII.</b>	<b>Appendix.....</b>	<b>35</b>

# I. Introduction

## 1.1. Subject analysis and motivation

The concept of addressing the sense of hearing for scientific reasons is not new, but has almost always been neglected in favor of methods using the sense of sight. This has happened for a variety of reasons, among them being the facts that quantitative calculations can be done and verified by viewing the data, thus leaving room for sight oriented analysis modes and technology to be developed and that the ear is an instrument used by most people to distinguish only qualitative auditory characteristics, often in an abstract way, therefore rendering it, initially, not usable for scientific research study.

In the particular case of seismology, the approach is no different, although significant progress has been made roughly in the last fifteen years. The main phenomenon studied in this scientific field, the earthquake, has properties that can be analysed both sonically and optically and more importantly, both individually and combined. One can easily conceive the prevalence of the eye in recognizing static situations, such as the current stress distribution in an area depicted on a graph or the dominance of the ear in identifying time dependent changes, e.g. the attack and release times of any triggered sound (an earthquake?) listenable. Nevertheless, the lack of technological means designed directly for sonic earthquake research raises the question: How and to what extent is resorting to auditory methods useful for seismological study?

Driven by these thoughts and by a more global interest in sound, an auditory investigation of earthquakes is attempted in this thesis. Various seismic records are audified and then processed with music production programs to extract results regarding two main subjects:

- i) The far-field Doppler effect in the Greek region caused by the 7/9/1999 M=5.9 Athens earthquake.
- ii) The anelastic attenuation phenomena in the Aegean Sea region studied for the intermediate depth 27/7/2006 M=3.3 Nisiros earthquake.

The sound files are available in the enclosed CD.

## 1.2. Brief history of auditory seismology

The first abstract reference to seismic sounds was possibly made by the Roman Stoic philosopher and statesperson Lucius Annaeus Seneca around 65 CE. It is written in the sixth book of his "Naturales Quaestiones", an encyclopedia of the natural world, that "prior to an earthquake, a roaring sound is often heard". Of course, that was merely an observation, but spatially in the course of history the value of audio-oriented approach in science is pointed out. Examples of this notion are found in the works of Pythagoras, Ptolemy and Johannes Kepler among others, where the natural laws that govern celestial bodies are investigated and discovered through the development of musical harmony and vice versa, giving birth to what is commonly referred to as the Music of the Spheres.

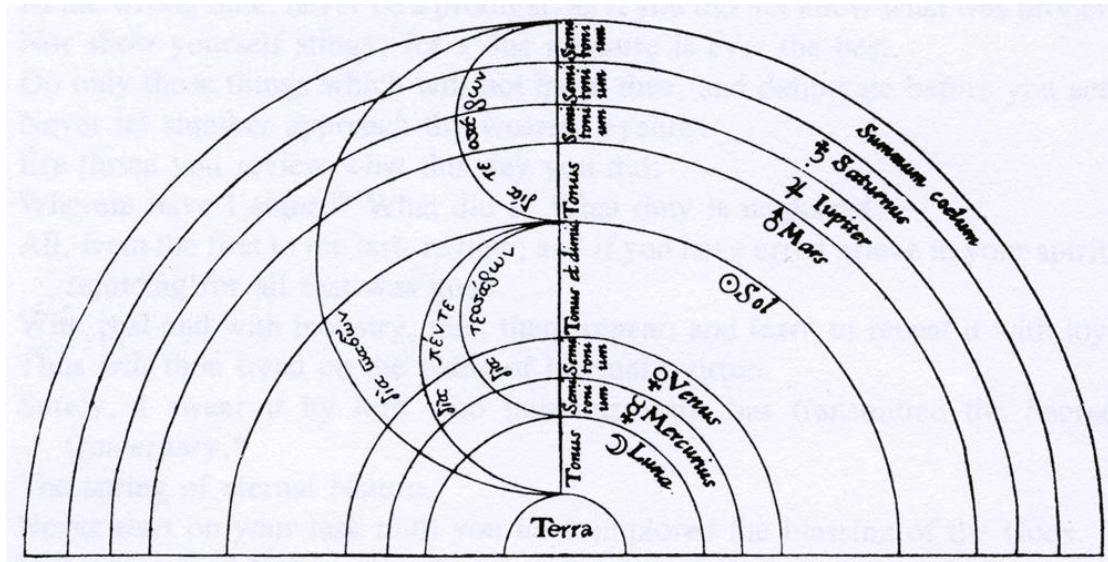


Fig.1: The Pythagorean notion of the correlation between musical intervals and the formation of the planets, as conceived in antiquity. (Image source: [www.american-budha.com](http://www.american-budha.com))

It was much later, in May 7th 1959, when Charles Percy Snow, an English chemist and novelist gave his famous and influential Rede lecture in Cambridge titled "The Two Cultures and the Scientific Revolution". In this lecture he discussed the fact that the intellectual world of the western society was split into two major cultures: the Sciences and the Humanities, which evolved totally independently from one another. From that point on, a fresher mindset was slowly beginning to grow in the academic world, affecting seismology as well.

Although the transformation of seismic data to audio had been accomplished at Caltech's Pasadena station on an early tape recorder by H. Benioff (1953), it was only in 1961, two years after the Rede lecture, that S.D. Speeth published

his paper named "Seismometer Sounds". In this publication, he used auditory methods to distinguish natural earthquakes from atomic explosions. G.E. Frantti and L.A. Leverault (1965) followed in the same direction. Muirhead and Simpson (1972) also recorded earthquakes and explosions in Australia using a direct recording tape system and employed time-shifting techniques in their processing. Part of their audio samples was incorporated in the "Interstellar Record" sent to space by NASA on the Voyager spacecraft in 1977.

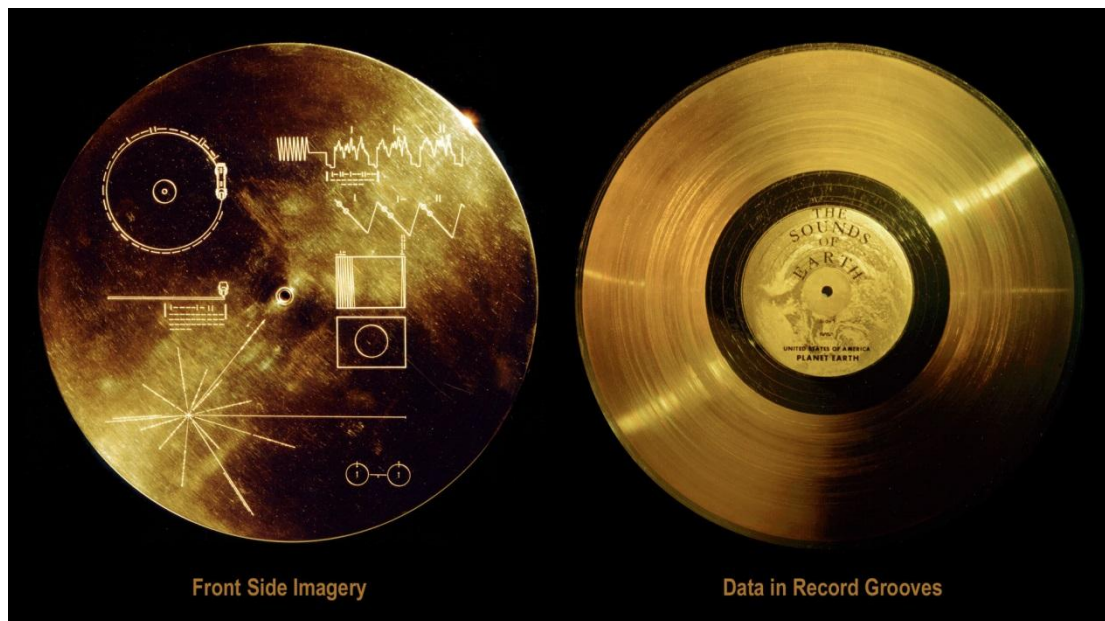


Fig.2: The Interstellar record. (Image source: russjamieson.com)

Since the last decade of the 20<sup>th</sup> century, much faster and wider progress has been made. C. Hayward presented a very sightful essay in 1992 about the capabilities of audified seismograms in seismic research in the International Community of Audified Research. Unfortunately, this effort was not significantly supported by the geophysical community. Frank Scherbaum (1999) also studied in depth the relation between seismic and sound waves through his work "The Earth as a Musical Instrument". Additionally, in collaboration with composer Wolfgang Loos, he audified volcanic seismic activity data and produced a music album named "Inner Earth, a Seismosonic Symphony".

Cellini, Mariotti and Nucera (2000) published a work on earthquake prediction using audification named "Fonosismologia, un approccio nuovo per l'analisi sismica", literally meaning "Phonoseismology, a new approach of seismic analysis". More recent notable papers include those of Florian Dombois on the use of audification in planetary seismology and seismology in general. He is the one of the scientists that coined the term "auditory

seismology". Through his work he attempts to embody audification as a basic tool in seismic research with very interesting results. He was also supervisor along with Stefan Wiemer and Oliver Brodewolf of the bachelor thesis of Eric Eberhard (2006) titled "Using audification to distinguish foreshocks and aftershocks". Andrew J. Michael (2011) and Zhigang Peng (2012) have also done important work on studying earthquakes through sound. Both Dombois and Peng are involved in the development of audification software programs for scientific, artistic and educational purposes. Hunstad et al. (2013) also contribute to this cause through their publication "Seismic waves and sound waves: from earthquakes to music".

Apart from his publications, Andrew J. Michael (1999) composed a musical piece called "Earthquake Quartet #1 for Voice, Trombone, Cello, and Seismograms". Following a similar artistic direction, Meier and Saranti (2013) converted seismic data to sound to create a composition named "Underground Sounds". Finally, Micah Frank uses different music production and virtual globe mapping programs to spot present earthquakes and create sounds from original audified seismic data in real time.

### **1.3. Methodology in outline**

For the needs of auditory processing, the seismic data underwent several transformations. The original miniSEED data was converted to ASCII files with the use of a Perl script, `Ms2ascii.pl`, available by UNAVCO in collaboration with IRIS. The ASCII files were then converted to WAV files using two MATLAB scripts written in the context of this study (see Appendix).

The first script reads ASCII converted Source Time Functions (STF) recorded in various stations, inverts the x and y axes and adds the inverted part to the original one to produce the full wavelength of a pseudo – periodic signal. This pseudo – periodic wave is then copied multiple times to create an array of itself (periodic function) and is saved in two versions in WAV format, rendering it listenable and with sufficient time duration to be clearly heard. The first copy is normalized to the maximum value of the file and the second copy is normalized to the maximum value of all examined STF files. The sample rate has been chosen at 8000 Hz (32 bits).

The second script reads ASCII converted seismic records of an earthquake recorded in different stations, its focal depth and the hypocentral distances between the focus and every single station. It then calculates the amplitude (equivalent volume) correction of each record according to the distance (as is

later explained in detail) and normalizes the records by reducing them to the same hypocentral distance. The average value of the geometrical spreading coefficient met for the distance correction is set to -1.7 for the Aegean subduction area (Skarlatoudis et al., 2013), hence the amplitude (volume) correction/normalization coefficient for each trace is calculated (in db) by

$$C = 17 \log_{10} \frac{R}{h} \quad (1)$$

where  $R$  is the hypocentral distance and  $h$  is the focal depth. After the normalization, each record is again saved twice in WAV format using the same approach as with the STFs. The sample rate for these files is chosen at 2500 Hz (32 bits). For the calculation of hypocentral distances, a third script is used that also computes the time delay of the arrival of the S waves after the P waves have arrived at each station. The earthquake that occurred in Nisiros in 27/7/2006 had an intermediate depth of  $h \simeq 120$  km and so, the arrival times of the P and S waves in seconds were calculated by the following relations (Ventouzi et al., 2013):

$$T_P = \frac{\sqrt{D^2 + h^2}}{7.62} \quad (2) \quad T_S = \frac{\sqrt{D^2 + h^2}}{4.27} \quad (3)$$

where  $D$  is the great circle distance between the epicenter and the recording station. The final processing of the WAV files was performed with the use of Ableton Live 8.2.2, a software music sequencer and digital audio workstation (see II and III).

## 1.4. Introduction to the main phenomena studied

### 1.4.1. Doppler effect

When a sound source and a listener engage in a relative motion, the sound frequency heard by the listener is not the original frequency of the source. The frequency perceived by the listener can be calculated and conclusions can be drawn about the movement direction of the source and/or the listener and also about their relative speed.

In seismology, one can also imagine the Doppler effect, where the sound source is the earthquake focus and the listeners are the earthquake recording stations. Nevertheless, there is a crucial difference: although relative motion between the two blocks of the seismogenic fault happens, there is no significant relative movement between the focus and the recording station. At the recording stations though, a frequency shift of the seismic waves that

arrive is observed. This happens mainly because of specific rupture conditions and also due to rock and tectonic environment changes that the seismic waves meet on their way from the focus to the recording stations (see fig. 5 and 6).

#### 1.4.2. Anelastic attenuation

When a seismic wave travels through a medium, part of the mechanical energy of the wave is gradually transformed into heat and at some point the wave is damped completely. This phenomenon is called absorption or anelastic attenuation.

Absorption mainly happens when the seismic wave meets grain boundaries, material and phase changes. It can be measured by a dimensionless parameter named seismic quality factor or  $Q$ , given by:

$$Q = 2\pi \frac{E}{\delta E} \quad (4)$$

where  $\frac{E}{\delta E}$  is the fraction of energy loss per oscillation cycle.

## II. Doppler effect

### 2.1. The Doppler phenomenon and its relation to seismology

As already mentioned, the Doppler effect is the natural phenomenon in which the frequency of any periodic event changes for an observer being in relative motion with the source. Typical examples of this are the frequency changes in the sound of a vehicle siren when it approaches and passes by an observer. When the vehicle approaches the observer, each successive wave is emitted from a position closer to the observer than the previous wave. Therefore, each wave takes slightly less time to reach the observer than the previous wave and the time between the arrivals of successive waves at the observer is reduced, causing an apparent increase in the frequency. While they are travelling, the distance between successive wave fronts is reduced and the waves assemble closer to each other. In the opposite case, when the vehicle is moving away from the observer, each wave is emitted from a position farther from the observer than the previous wave, so the arrival time between successive waves is increased, reducing the frequency. The distance between successive wave fronts is increased, so the waves "spread out". Supposing the observer is stationary and that the speed of the vehicle (source) is lower than the velocity of sound in the medium, the relationship between the frequency emitted and the frequency perceived is given by:

$$f = \left(\frac{c}{c+v_s}\right)f_o \quad (5)$$

where  $f$  is the frequency perceived by the receiver,  $f_o$  is the frequency emitted at the source,  $c$  is the velocity of waves in the medium and  $v_s$  is the speed of the vehicle (source). If the source approaches the observer, the source speed has a negative sign and if it moves away from the observer, it has a positive sign.

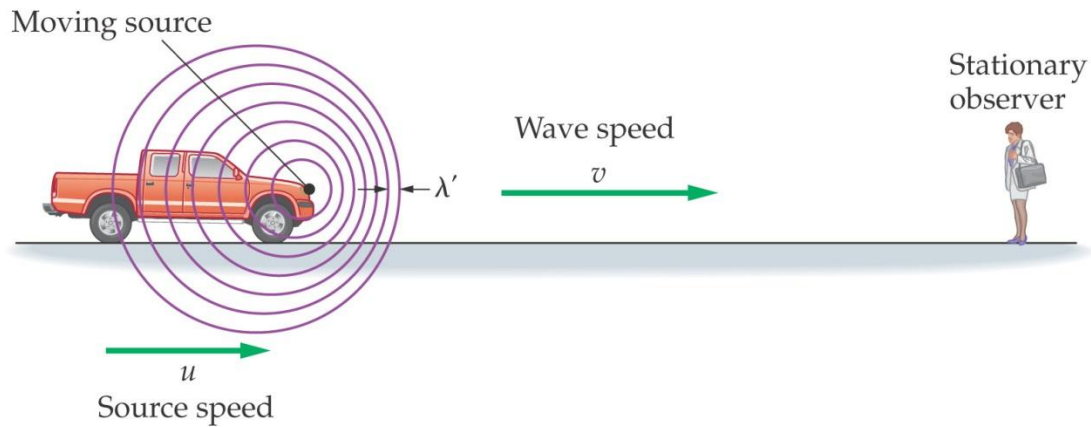


Fig.3: The Doppler effect for a moving source and a stationary observer. (Image source: user.physics.unc.edu)

In the case of a stationary source and a moving observer, the concept of relative motion and frequency perception remains the same. Again, supposing that the speed of the observer is lower than the velocity of waves in the medium, the relationship between the frequency emitted and the frequency perceived is given by:

$$f = \left(\frac{c+v_r}{c}\right)f_o \quad (6)$$

where  $f$  is the frequency perceived,  $f_o$  is the frequency emitted,  $c$  is the velocity of waves in the medium and  $v_r$  is the velocity of the receiver (observer). If the observer approaches the source, the observer speed has a positive sign and if he moves away from the source, it has a negative sign.

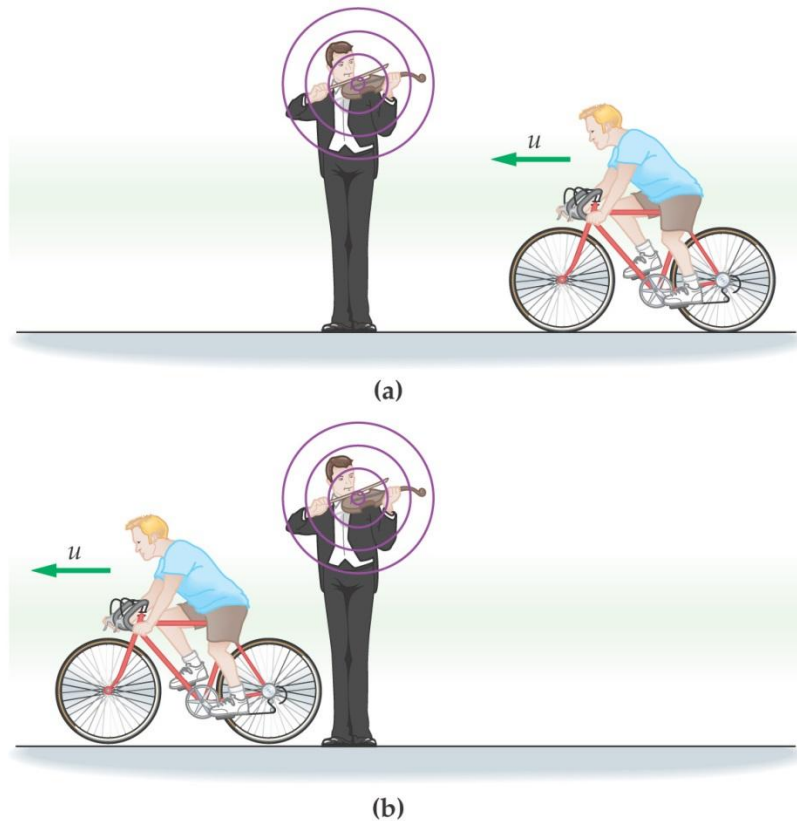


Fig.4: The Doppler effect for a stationary source and a moving observer. (Image source: user.physics.unc.edu)

If the source and the observer engage in a motion moving both relative to each other, (5) and (6) can be generalized into one equation which is:

$$f = \left( \frac{c+v_r}{c+v_s} \right) f_o \quad (7)$$

where all variables are as explained before. It is easily understood that the frequency perceived is increased when either the source or the observer (or both) are moving towards one another and that it is decreased when they are moving away from one another. It is also important to note that the equations cited above explain the phenomenon supposing that the relative motion is taking place in a straight line between the source and the observer, that is, the angles between the speed vectors and the straight line connecting the source and the observer are zero.

To understand the relation of the Doppler effect to seismology, a reference to the nature of ground motions is necessary. Earthquake ground motions are affected by three factors: (i) the source effect, which is a manifestation of the non-uniformity of the seismic waves produced at the focus, (ii) the path effect, which corresponds to the modifications the seismic waves undergo during their propagation through the media until they reach the recording site and

(iii) the local site effect, which reflects the alteration of the seismic waves due to the characteristics of the soil formations of the recording site.

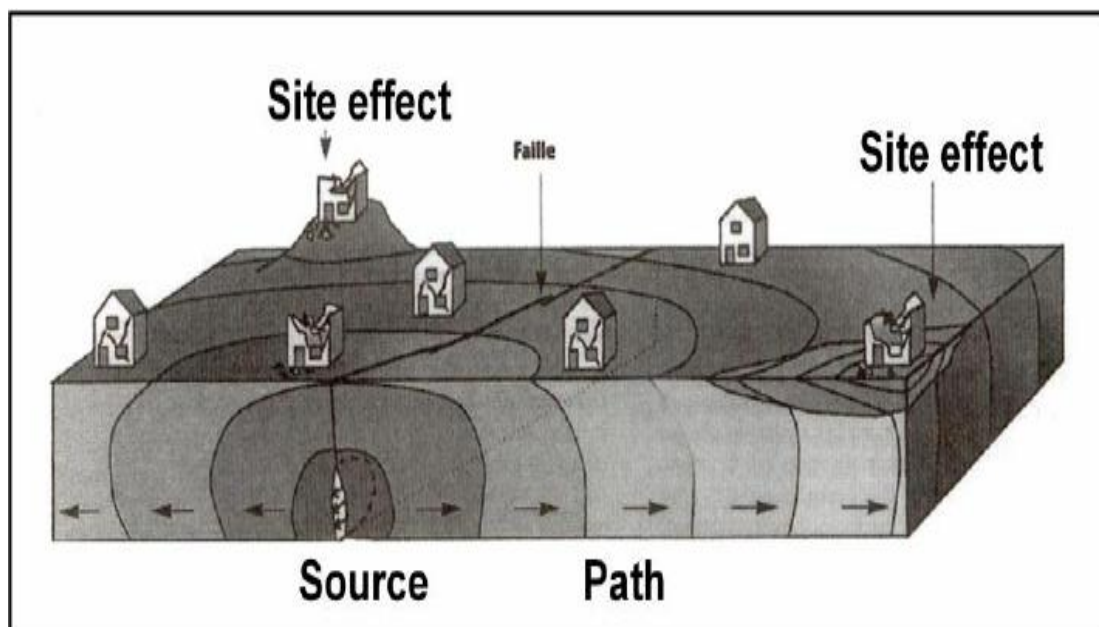


Fig.5: The various ground motion effects. (Image source: commons.wikimedia.org)

As mentioned in 1.4.1., the causes of the earthquake Doppler effect primarily derive from rupture conditions of the seismogenic fault. These conditions are expressed through the rupture directivity effect, which is essentially a manifestation of the Doppler effect in the direction parallel to the orientation (strike) of the fault. It occurs when the rupture velocity is close to the wave velocity of the rock mass near the source. Supposing there are two sites bilaterally placed near a shear zone, if a rupture happens, the site being in the direction of it receives seismic waves “compressed” in time. This is expressed by large amplitude and a small duration pulse recorded in the site’s seismographs. In the opposite site, the received waves “expand” in time, resulting in smaller amplitude and a long duration pulse recorded in the site’s seismographs. The path effect also plays a passive role in the manifestation of the earthquake Doppler effect by forcing waves to arrive in different times to the sites, following Snell’s law and Fermat’s principle in case they pass through different geological formations and/or tectonic structures such as faults, folds, joints etc. The same goes with the local site effect. Nevertheless, since there is an energy loss per cycle during the propagation of seismic waves, the path effect and the site effect play a more important role in the attenuation mechanism and so they are studied at larger extent in chapter III.

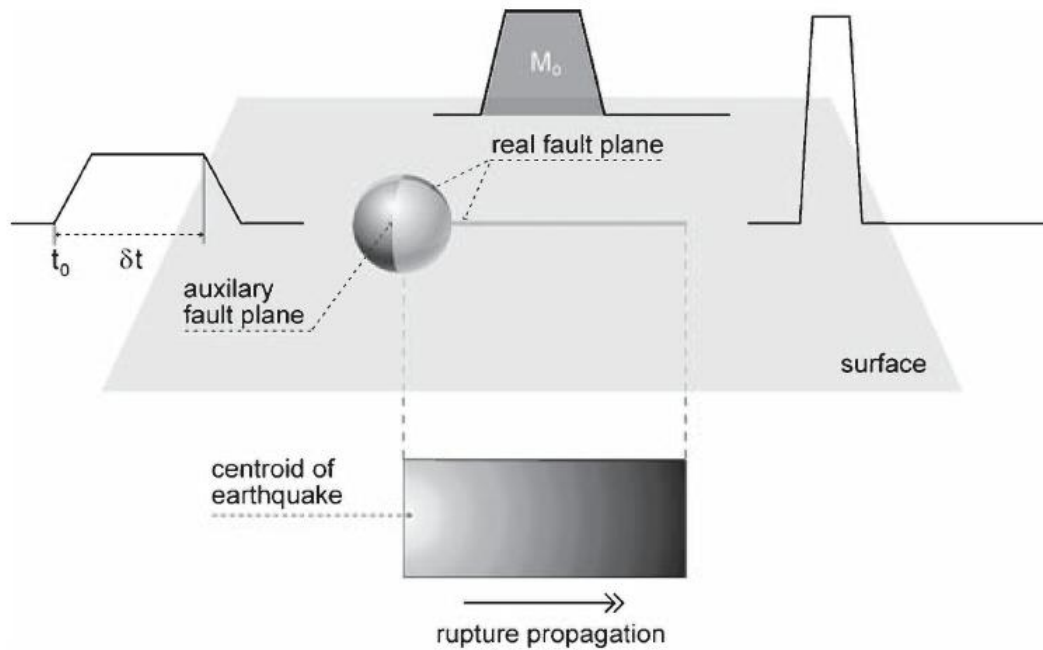


Fig.6: The rupture directivity effect. (Image source: seismo.snu.ac.kr)

## 2.2. Sound processing of Doppler data from the 7/9/1999 M=5.9 Athens earthquake

### 2.2.1. General information about the seismic event

On September 9 1999 a moderate size earthquake of magnitude  $M=5.9$  took place a few kilometers outside the city center of the capital of Greece, Athens. It caused serious damage, an unexpected occurrence because of its moderate size, especially in the north - northwest suburbs of the city, with 43 people deceased and 2000 injured in 30 collapsed buildings, both industrial and residential. The extensive damage caused in the N – NW part of the city is partially attributed to local soil conditions and topographic relief, but synthetic calculations also imply the occurrence of rupture directivity effects. The earthquake triggered 15 accelerographs in a radius of 30 kilometers from the epicenter, but none of these instruments were installed within the meizoseismal area. Source time functions of the mainshock were estimated by the deconvolution of broadband body waves from a nearby smaller event with similar focal mechanism using an empirical Green's function (Roumelioti et al., 2002). As explained in 1.3., this STF data have been converted to sound samples in order to study the Doppler effect caused by this earthquake using an auditory approach and to investigate whether the

results found following this method match the previous results. The data conversion and processing are explained in detail below.

### 2.2.2. Data extraction and conversions

The original data collected were recorded by the national broadband network operated by the National Observatory of Athens. The geographical distribution of the stations is shown in Fig.7 where it is clear that the largest azimuthal gap between two consecutive stations is about 60°. This is important for the processing method which is explained in 2.2.3..

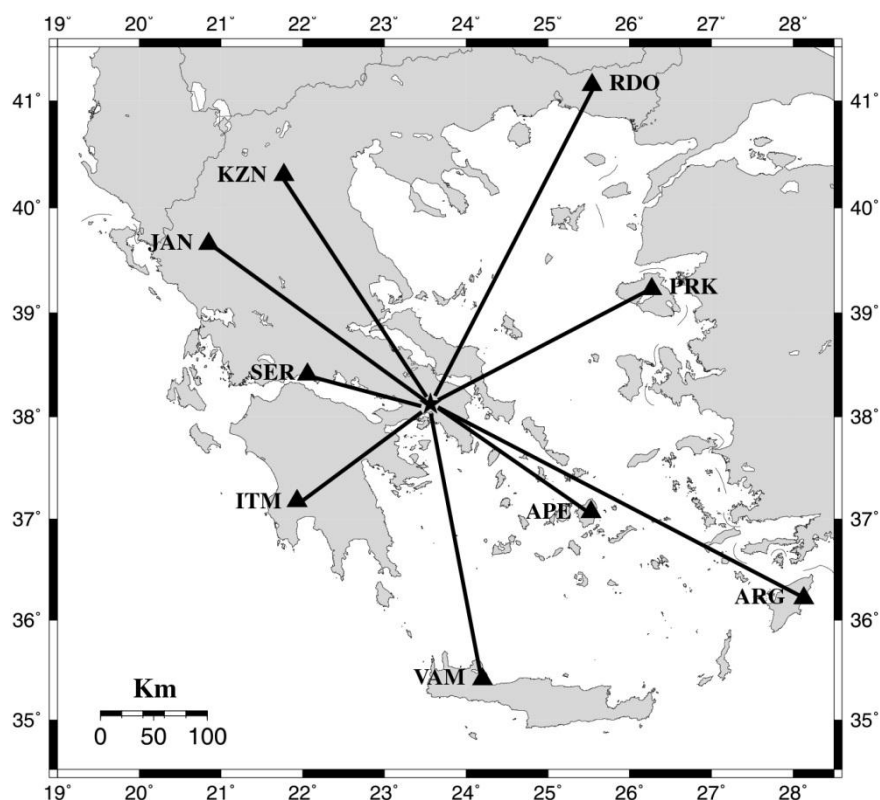


Fig.7: Map showing the location of the different stations used for the accumulation of the STF data with respect to the epicenter of the Athens earthquake. (Roumelioti et al., 2002)

For the production of the STF data, the following process was employed (Roumelioti et al., 2002): In the frequency region and in the case of a point source, the far – field displacement,  $U(\omega)$  recorded at distance  $r$  and azimuth  $\varphi$  is given by

$$U(\omega) = \dot{M}(\omega)G(\omega, r, \varphi)RI(\omega) \quad (8)$$

where  $\dot{M}$  is the source time function of the event,  $G$  is the Green's function response of the medium along the wave path, including geometrical spreading and attenuation effects,  $R$  is the radiation pattern factor and  $I$  is the

response of the recording instrument. In order to extract the STF from the displacement records, the propagation path and recording instrument effects have to be removed. This can simply be done by deconvolving the waveforms of a nearby smaller event with similar focal mechanism, resulting in the empirical Green's function (eGf) mentioned before. In this procedure, the small event is hypothesized to be a point source in space and time, and to the degree that this supposition is not valid, the STF of the studied event will be a relative approximation to the STF of the small event. Consequently, the eGf will be both small enough to be approached as a point source and large enough to provide a decent signal – to – noise ratio at the investigated distances. The estimated STF is then normalized to unit area so as to correct the amplitudes due to differences in radiation patterns between the eGf and the mainshock and to ensure that all the STF are reduced to the proper scalar seismic moment.

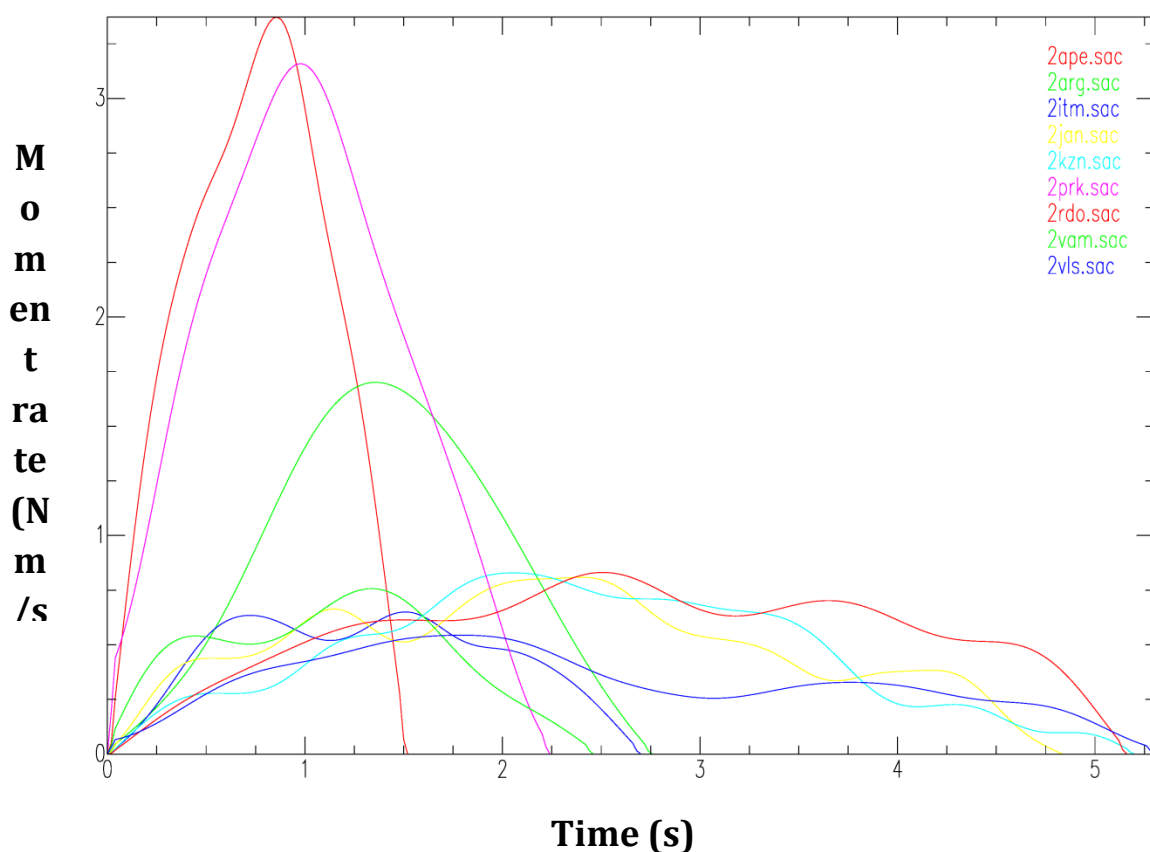


Fig.8: The STF normalized to unit area. The station SER is replaced by VLS, a station nearby SER, for data availability reasons. (Modified from Roumelioti et al., 2002)

As explained in 1.3., the STF data is transformed into ASCII files using a Perl script, Ms2ascii.pl, available by UNAVCO in collaboration with IRIS. The ASCII files then undergo further conversions with the aid of a MATLAB script (see Appendix). Each ASCII file corresponding to a single STF is

scanned for the maximum amplitude value of all the files. Subsequently, the STF is inverted in the x and y axes and the new wave part is added to the tail of the original one. Thus, a complete 'artificial' wave is created. The maximum amplitude value of the STF itself (local) is then determined and the wave is later replicated 100 times resulting in a pseudo – sinusoidal waveform which is saved in WAV format twice: the first WAV file being normalized by the maximum amplitude value of all the files and the second WAV file being normalized by its local maximum amplitude value. These files are saved using a sample rate of 8000 Hz (32 bits), which means for the available data that the shortest file has a duration of about 1 second and the longest file has a duration of about 7 seconds.

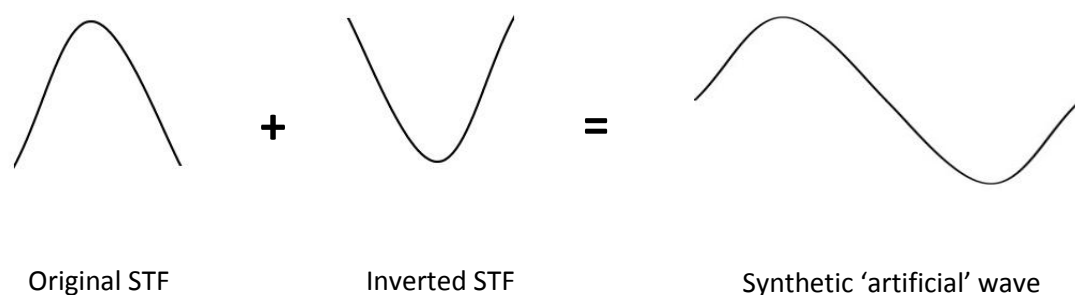


Fig.9: Schematical representation of the complete 'artificial' wave construction process. Both axes become subjects of inversion regarding the inverted STF. (The dimensions of the resulting wave are distorted in this image.)

### 2.2.3. Data processing

For the WAV data processing, Ableton Live 8.2.2. was employed. This is a music making software which is very versatile and useful for recording, arranging, mixing and mastering, among others. The WAV files were imported in four Live sets, clockwise from station RDO, as follows:

- i) The first Live set (track 1 titled 'Athens Doppler local – L') including the WAV files normalized by their local maximum value and with their original duration retained.
- ii) The second Live set (track 2 titled 'Athens Doppler local – S') including the WAV files normalized by their local maximum value and with the duration of each file adjusted to about 1 second.
- iii) The third Live set (track 3 titled 'Athens Doppler uni – L') including the WAV files normalized by the maximum value of all the files and with their original duration retained.

- iv) The fourth Live set (track 4 titled 'Athens Doppler uni – S') including the WAV files normalized by the maximum value of all the files and with the duration of each file adjusted to about 1 second.

The first two tracks correspond to the STFs as were initially normalized to unit area. In the first track, the multiplication by 100 is kept intact in order to represent both the wave lengths and the frequencies, while in the second track only the frequencies are kept intact, so as to render quicker a pitch comparison. In the last two tracks, the unit area normalization is cancelled, hence an amplitude (volume) comparison becomes possible. Again, in the third track, the multiplication by 100 is kept intact and we can perform a comparison of wave lengths (duration), frequencies (pitch) and amplitudes (volume), whereas in the fourth track, only frequency and amplitude comparisons are possible.



Fig.10: Track 1 WAV files as imported in their Live set. The waveforms are not clearly visible since they have been compressed to fit in the image.



Fig.11: Track 2 WAV files as imported in their Live set. The waveforms are not clearly visible since they have been compressed to fit in the image.



Fig.12: Track 3 WAV files as imported in their Live set. The waveforms are not clearly visible since they have been compressed to fit in the image.



Fig.13: Track 4 WAV files as imported in their Live set. The waveforms are not clearly visible since they have been compressed to fit in the image.

By playing the tracks, an audified azimuthal distribution of the STF's is heard. It is clear in all of them that stations PRK, ARG and APE received high frequency waves, while VLS, JAN and KZN received low frequency waves meaning that the rupture directivity had a NW – SE direction. This observation is in accordance with the fact that the greater amount of damage in the metropolis of Athens due to the earthquake happened in the NW part of the city. The STF azimuthal propagation patterns become even clearer listening to the third and fourth tracks where the differences in volume reflect the relative amplitude proportions.

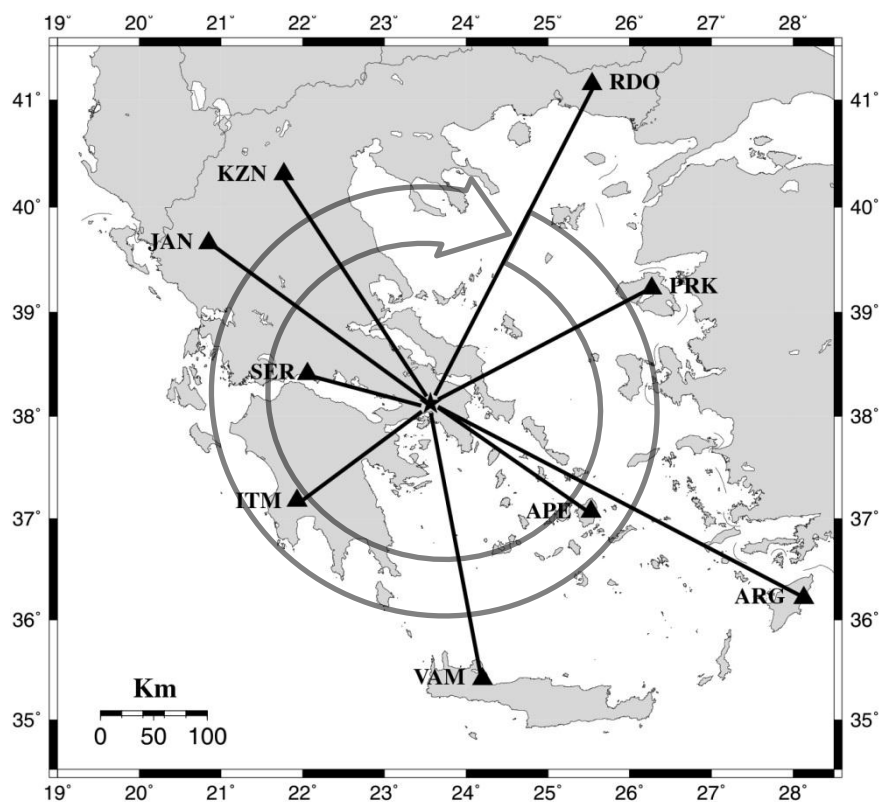


Fig.14: Map showing the playback order of the STF's (clockwise from RDO station) in tracks 1 – 4, representing the audified STF azimuthal distribution. (Modified from Roumelioti et al., 2002)

### III. Anelastic attenuation

#### 3.1. Attenuation types of seismic energy

The amplitudes of elastic waves recede as they travel through a medium which means that elastic waves attenuate during their propagation. This attenuation is divided into two types:

- i) Scattering (elastic attenuation)
- ii) Absorption (anelastic attenuation)

Scattering or geometric scattering is the distribution of energy to greater material volumes. If there is a point energy source and the energy is distributed spherically, the energy fraction  $\delta W$  passing through two different spherical surfaces in the fraction of time  $\delta t$  will be the same. If  $r_o$  and  $r$  are the radii of the spherical surfaces and  $I_o$  and  $I$  the respective intensities of the waves passing through them,  $I$  is given by:

$$I = I_o \frac{r_o^2}{r^2} \quad (9)$$

and since

$$I = kA^2 \quad (10)$$

the amplitude  $A$  is given by:

$$A = A_o \frac{r_o}{r} \quad (11)$$

where  $A$  and  $A_o$  are the respective amplitudes for radii  $r$  and  $r_o$  and  $k$  a value that is a function of propagation medium density, wave velocity and wave frequency. It is obvious from (11) that the amplitude variation is inversely proportional to the distance.

As was mentioned before, in the study of geometric scattering it is supposed that as the energy propagates through two successive spherical surfaces, there is no energy loss and that the amplitude simply decreases due to the distribution of energy to even larger space as time passes. However, part of the wave energy is actually gradually transformed into heat by the propagation medium, causing the ground oscillations to eventually fade out completely. This phenomenon is called absorption.

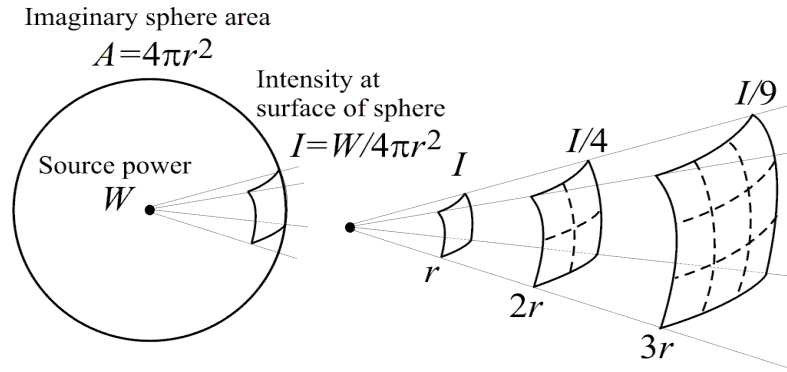


Fig.15: The attenuation mechanism of geometric scattering. (Image source: resource.isvr.soton.ac.uk)

The exact mechanism causing the transformation of elastic wave energy into heat is not known, but phenomena of internal friction in the solid propagation media and viscous friction in the fluids filling the pores of rocks, contribute effectively, among others (piezoelectric and thermoelectric phenomena, energy consuming for the creation of new surfaces in the process of rock fracture etc.) to the attenuation of elastic waves. In a first approximation, it is accepted that anelastic attenuation changes exponentially with the distance. If  $I_0$  is the intensity at a point  $P$  near the focus of the wave and  $I$  is the intensity at a distance  $r$  from  $P$ ,  $I$  is given by:

$$I = I_0 e^{-Qr} \quad (12)$$

where  $Q$  is the seismic quality factor given by (4). The seismic quality factor increases with the wave frequency and, in a first approximation, can be considered proportional to it. This is the reason why high frequency elastic waves attenuate intensely with the distance. Equations (9) and (12) are usually combined into one that has the form of:

$$I = \frac{I_0}{r^2 e^{Qr}} \quad (13)$$

which combined with (10) gives:

$$A = \frac{A_0}{r e^{\frac{Qr}{2}}} \quad (14)$$

Experimental data show that the attenuation of elastic waves due to geometrical scattering is stronger than that of anelastic absorption for small distances, while as the distance and/or the frequency of the waves increase, the anelastic absorption increases and eventually (for long distances and/or high frequencies) becomes the mechanism that completely defines attenuation.

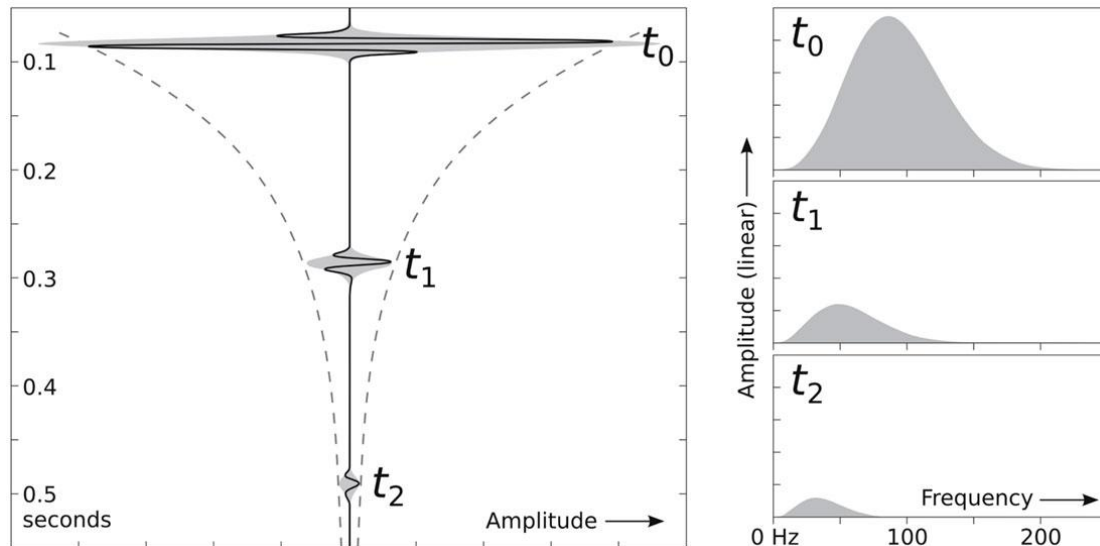


Fig.16: The attenuation mechanism of absorption. (Image source: csegrecorder.com)

### 3.2. Active tectonics and anelastic attenuation in the Aegean region

The geological setting of the Aegean Sea consists of an active tectonic plate boundary environment (Hellenic Arc). The collision of the African plate with the Eurasian plate occurs with a velocity of  $\sim 1.0$  cm/yr in the N-S direction, while the movement of the Aegean lithosphere overriding the African plate happens with much greater velocity ( $\sim 3.5 - 4.0$  cm/yr) in the NE-SW direction (Papazachos C., 1999). Thrust fault interface earthquakes are found at depths of 30 – 60 km in the Hellenic Arc and oblique – thrust in – slab earthquakes occur in the Wadati – Benioff zone at intermediate depths ranging from 60 – 170 km (Papazachos and Komninakis, 1969; LePichon and Angelier, 1979). The foci of intermediate – depth earthquakes (those whose foci are placed at 45 – 300 km beneath the Earth’s surface) form two segments of the southern Aegean Benioff zone with distinct dipping angles. The shallower segment, including focal depths around 45 – 90 km, has a low dipping angle and corresponds to the outer part of the Benioff zone. The deeper segment, including focal depths around 90 – 160 km, corresponds to the inner part of the Benioff zone and plunges steeply underneath the southern Aegean volcanic arc (Papazachos, 1990; Papazachos et al., 2000). The back – arc location shows very low levels of ground motion for intermediate – depth

seismic events (Papazachos and Komninakis, 1971) and the southern border of this belt coincides with the volcanic arc, revealing a relationship between the attenuation patterns and the presence of the volcanic arc and the associated mantle wedge in the area (Papazachos et al., 2005; Boore et al., 2009; Skarlatoudis et al., 2009).

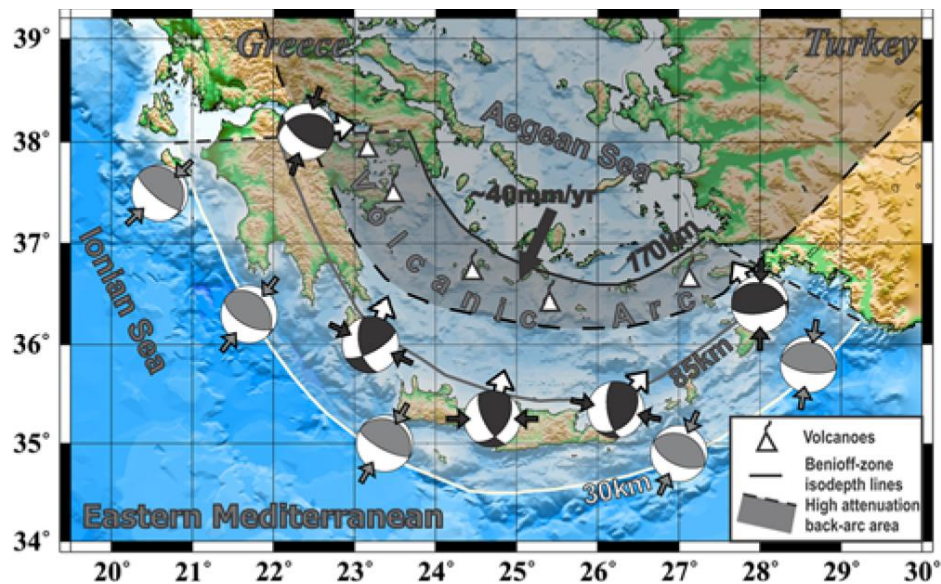


Fig.17: The Hellenic arc subduction setting and the corresponding Benioff zone. (Skarlatoudis et al., 2013)

The highly complicated structure of the Greek subduction zone results in the variation of the seismic wave propagation paths from the source to the surface, depending on the earthquake type (interface, in – slab or crustal) and recording site (Skarlatoudis et al., 2013). Different types of earthquakes produce ground motions recorded diversely at various sites, even for events having the same magnitudes and hypocentral distances. By the works of many researchers (e.g., Papazachos and Komninakis, 1971; Konstantinou and Melis, 2008; Boore et al., 2009; Skarlatoudis et al., 2013) it has been found that the back – arc area of the Northern – Central Aegean exhibits high attenuation response to intermediate – depth seismic events, while in the area of subduction, a low attenuation pattern is observed. In – depth study of the wave propagation patterns in the Hellenic Arc reveals that along the subducting slab, both interface and in – slab seismic events are generated. Seismic waves originating from shallow in – slab events propagate along the Aegean lithosphere without any differentiation, as it is shown in the records of stations in short distances from both inner – arc and outer – arc regions. At larger distances from the Hellenic trench, the waves demonstrate a more complex behavior: they either travel through the high  $Q$  subducting slab towards the outer arc, and therefore are amplified, or pass through the low  $Q$  mantle wedge below the volcanic arc, hence being attenuated. This back -

arc/along - arc contrast becomes clearer as hypocentral distances increase and at a certain point, the waves travel through the whole mantle wedge area, resulting in no further enhancement of the attenuation at more remote stations. For seismic events occurring at depths greater than 100 km in the second Benioff zone segment, the back - arc/along - arc contrast is observable for all records, as the seismic waves are bound to travel through either the subducting slab or mantle wedge area. Since the mantle wedge has specific dimensions, all waves travel the same distance in the low  $Q$  area for hypocentral distances greater than 100 km, and beyond that depth, the back - arc/along - arc contrast remains the same (Skarlatoudis et al., 2013)

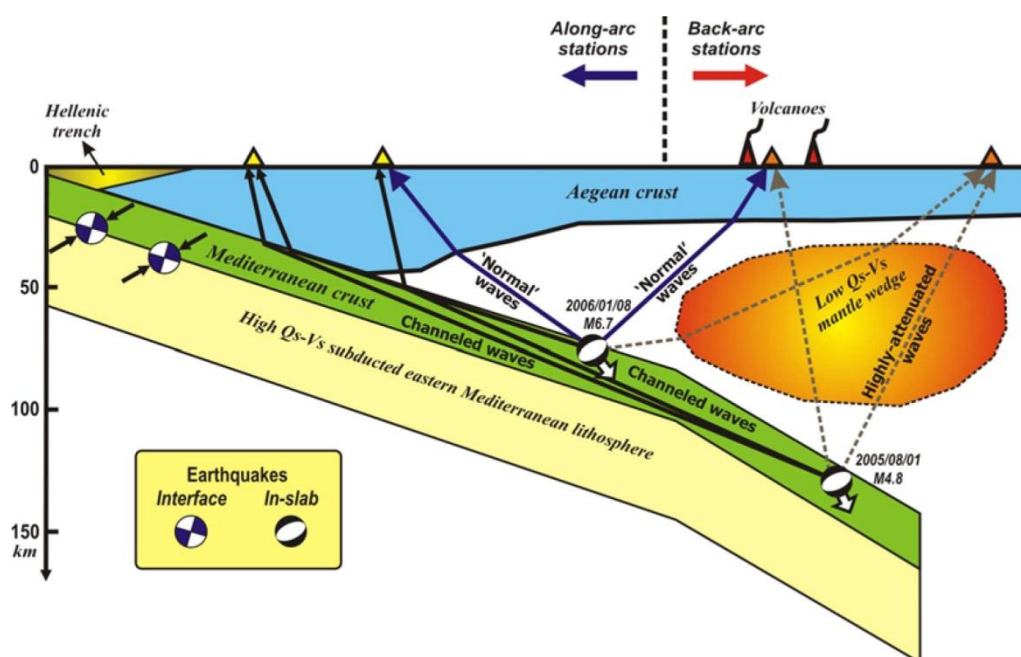


Fig.18: Seismic wave propagation and attenuation patterns in the Hellenic Arc. (Skarlatoudis et al., 2013)

### 3.3. Acoustic study of the intermediate depth 27/7/2006 M=3.3 Nisiros earthquake

#### 3.3.1. General information about the seismic event

For the acoustic study of anelastic attenuation through the seismic activity of the Hellenic Arc, a seismic event with specific properties had to be chosen. Initially, it was necessary that the earthquake had a significant magnitude in order to be clearly recorded in stations both in the back - arc and along - arc areas. Moreover, it should be an earthquake with its epicenter placed somewhere in the central Aegean region, so as to reveal the Benioff - zone attenuation patterns and to distribute the stations with equally strong records,

although normalizations were executed. Thirdly, its focal depth had to be greater than 100 km so that the waves were bound to cross the whole tectonic structure of the subducting slab and mantle wedge and to catch the full extent of the along – arc/back – arc attenuation bias. The chosen earthquake seemed to fulfill all the requirements, since it had the adequate magnitude of  $M=3.3$ , its epicenter was located a few kilometers west of the island of Nisiros and its focal depth was calculated at  $\sim 120$  km (intermediate depth).

### 3.3.2. Data extraction and conversions

The seismic data used were recorded by stations of the EGELADOS working group, although due to the magnitude of the earthquake, it was also recorded by the permanent station network. The extracted data consists of Z (vertical) component records from six stations, three in the back – arc area (FOLE, AMOS, KOSI) and three in the along – arc area (ZKR, KAPA, RHOS). The Z component records have been chosen because the study target is to audify the anelastic attenuation mechanisms primarily in the vertical direction, that is, as the seismic waves penetrate the Hellenic Arc tectonic structure at different depths. The selection of stations also provides insight for the attenuation pattern, since half of the stations are located directly above the outer - arc subduction interface and the others are located in the volcanic arc and directly above the mantle wedge.

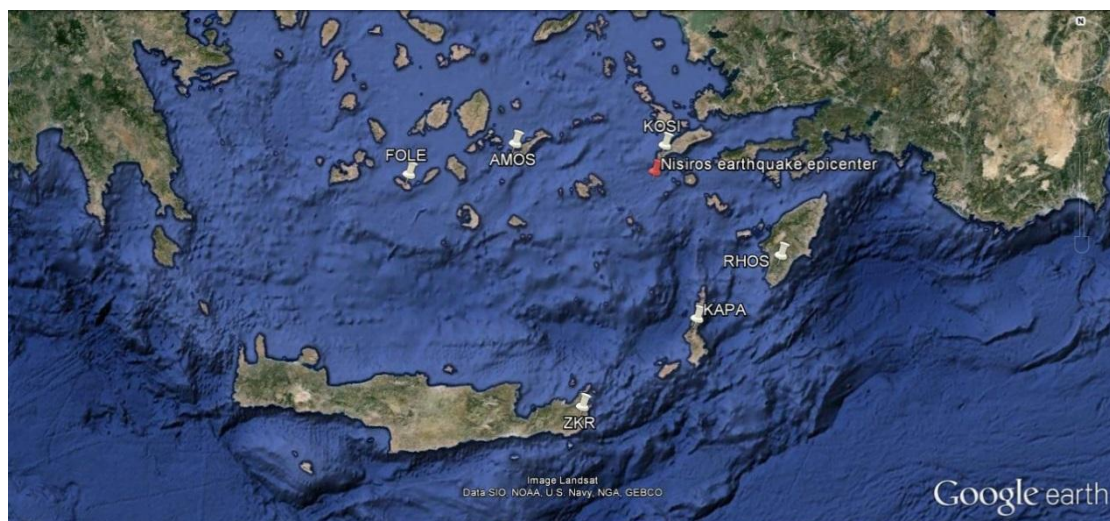


Fig.19: The station distribution of the extracted data with respect to the 27/7/2006  $M=3.3$  Nisiros earthquake epicenter.

The data conversions were executed in a manner similar to that of the STF data mentioned before. The original recordings were converted to ASCII files and then, those files were sonificated via a second MATLAB script (see

Appendix). The script reads the ASCII files, the respective calculated hypocentral distances of the original recordings and the focal depth ( $h=120.66$  km). It then calculates the amplitude (volume) correction coefficient according to the distance, given by (1) and also retrieves the local maximum amplitude value of each file and the maximum amplitude value of all the files. The volume correction applied in dBs is given by:

$$Cor_{dB} = 10\log_{10}(C) \quad (15)$$

where  $C$  is the correction coefficient given by (1). The files are then saved in WAV format, once normalized by their local maximum value and once by the maximum value of all the files. The sample rate conversion is chosen at 2500 Hz (32 bits) which gives the WAV files a time duration of about 7 seconds. For the calculation of hypocentral distances, another short MATLAB script is used that reads the epicenter and recording station coordinates, computes the great circle distance between them and extracts the corresponding hypocentral distances.

### 3.3.3. Data processing

The WAV data are once again imported to Ableton Live 8.2.2. for processing and two Live sets are created. The first Live set includes the local maximum amplitude value corrected WAV files and the second Live set includes the WAV files corrected by the maximum amplitude value of all the files (tracks 5 – 16). Each WAV file in the two sets is accompanied by its respective FFT spectrogram, so as to view the frequency changes at the arrival times of the P and S waves. The P and S wave arrival times are also calculated in the last MATLAB script mentioned before by the equations (2) and (3), as well as their estimated time difference. Since the WAV files are saved at a sample rate of 2500 Hz and the original records had a sample rate of 100 Hz, the P and S travel times for the WAV files in seconds are given by the modified equations:

$$TWAV_P = \frac{\sqrt{D^2+h^2}}{7.59} 0.04 \quad (16) \quad TWAV_S = \frac{\sqrt{D^2+h^2}}{4.27} 0.04 \quad (17)$$

where  $D$  is the great circle station - epicenter distances and  $h$  is the focal depth.

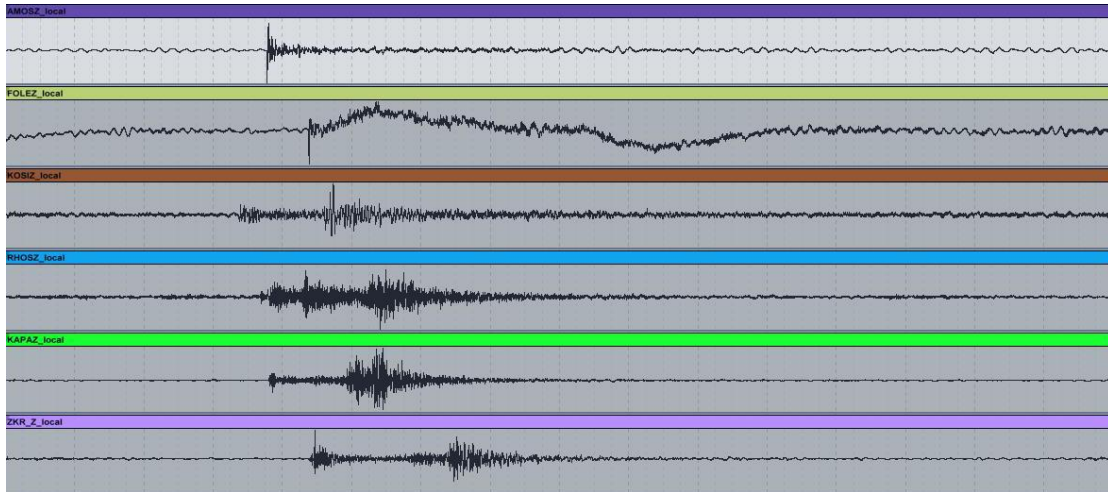


Fig.20: The selected waveforms of 27/7/2006 M=3.3 intermediate depth Nisiros earthquake, normalized by the local maximum amplitude value of each file.

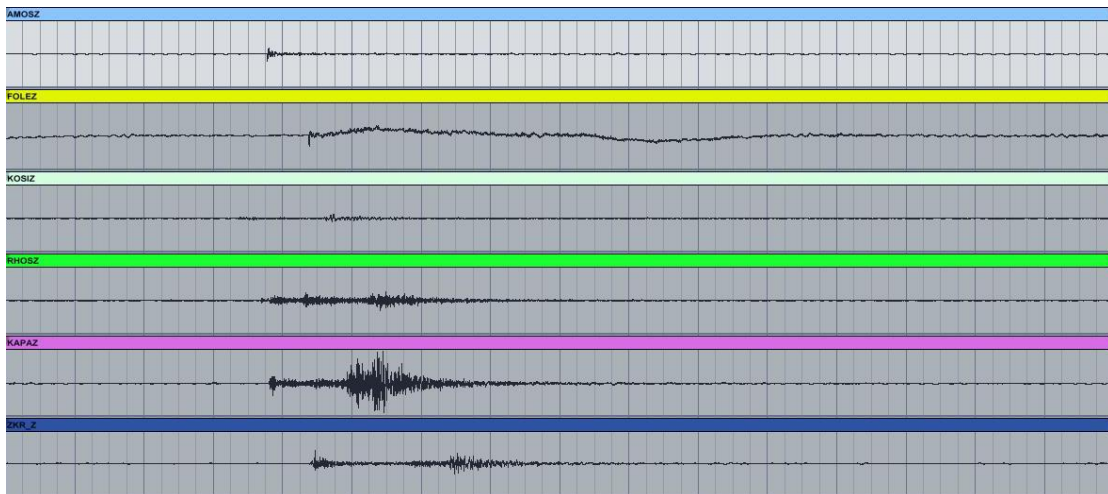


Fig.21: The selected waveforms of 27/7/2006 M=3.3 intermediate depth Nisiros earthquake, normalized by the maximum amplitude value of all the files.

From equations (16) and (17) the arrival time differences have been calculated by subtracting the corresponding results. The outcome of this subtraction practically reflects the arrival delay of the S waves after the P waves have arrived to the recording station. This delay can sometimes be accurately calculated by simply looking at the waveforms; however this is a special case since the waveforms are usually complex and both the background noise and the arrived P waves constitute the noise for the S waves, making it difficult to spot the S pulse onset. The S wave arrival delay can also be heard in the WAV files and a very useful function of Ableton Live 8.2.2 is that it can playback the sound data at different speeds without altering the pitch, hence making it easier to accurately spot any desired time moment in a sound sample. The S

wave arrival delay times calculated addressing all the aforementioned methods are presented in Table 1 below.

**Table 1**

Numerically (using equations 16 and 17), visually and audibly calculated S wave arrival delay times. Notice that the estimated delays correspond to the final WAV files, after frequency resampling

<b>Station</b>	$(T_S - T_P)_M$ (sec)	$(T_S - T_P)_O$ (sec)	$(T_S - T_P)_A$ (sec)
<b>FOLE</b>	0.872	0.899	0.882
<b>AMOS</b>	0.611	0.691	0.747
<b>KOSI</b>	0.502	0.547	0.587
<b>ZKR</b>	0.881	0.898	0.928
<b>KAPA</b>	0.705	0.513	0.528
<b>RHOS</b>	0.668	0.665	0.699

## IV. Discussion

The audified data provided interesting information about both the earthquake Doppler effect and the anelastic attenuation study, but in order to render the audified data useful for research, the most crucial process was that of original data conversions. Attention was paid to the conversion process, so as to maintain the data properties carrying physical information. Applying the same conversion to all the data was also necessary for comparison. In the case of the STFs, the parallel synthesis and conversion of the data didn't distort the physical information content, but made the acoustic study more clear. Indeed, the differences in pitch and in duration of the synthetic waveforms combined gave an unambiguous impression of the nature of directivity phenomena. The playback order according to the azimuthal distribution of the audified STFs also aided the understanding of these phenomena significantly by including the geographical setting. On the other hand, the (de)normalization of the STFs by the maximum amplitude value of all the files didn't seem to be very useful, since the normalization to unit area was retracted by it and some audified files were hard to be heard at all.

For the Nisyros earthquake audified recordings interpretation, a much deeper analysis is imperative. From a preliminary audio listening, it is evident that stations FOLE, AMOS and KOSI recorded attenuated seismic waves, while ZKR, KAPA and RHOS recorded amplified seismic waves. This is implied by the low pitch and also by the almost indistinguishable S wave arrivals in the first three recordings, contrary to the other three recordings, where the pitch is relatively higher and the S wave arrival times are distinct. Additionally, in the case of the Nisiros earthquake audified data, the normalization by the maximum amplitude value of all the files seemed to be very useful for the acoustic representation of the anelastic attenuation patterns, since it provided a more pronounced and complete notion of the relative differences between the attenuated waves in the back – arc area and the amplified waves in the along – arc area of the Hellenic Arc. This amplitude (volume) comparison capability was not available in the study of the audified files that were normalized by the local maximum amplitude value.

Additional conclusions can be drawn by considering the differences found in the extracted S wave arrival time delays, calculated by the three methods presented before. One would argue that numerical estimations (based on the closed formula relations, which are calibrated on real traveltime arrival data) produce the most reliable results, but in many cases this is false for a variety of reasons. Firstly, the equations used for the prediction of seismic wave

arrival times take into consideration only the great circle paths and the focal depths and ignore the path effects. Secondly, the complexity of the waveforms can sometimes blur the S wave arrival times, or even the P wave arrival times when there is too much background noise, making the numerical estimations almost impossible to verify. Although the results presented in table 1 are in general agreement, the subtle deviations shed light to the strengths and weaknesses of each method. The visually determined S wave arrival time delays were easy to calculate for stations ZKR, KAPA and RHOS (and KOSI at less robust level), since the rapid enhancement of amplitudes made the wave arrivals clearly observable. Nevertheless, visual calculations were very difficult in the cases of stations FOLE and AMOS and especially for FOLE, where the presence of a slow carrier wave rendered the S waves almost invisible.

Similar analysis characteristics were met in the acoustic approach. In most cases, the P and S wave arrival times were impressive to hear and for the stations located in the along – arc area, the arrival times were easy to calculate with satisfactory accuracy. For the stations located in the back – arc area (excluding KOSI), the S wave arrivals were difficult to hear due to loud background noise and high attenuation, hence those calculations are less reliable. Observing Table 1, one can see that the estimated times determined audibly are slightly slower than those calculated optically and that is because, for fast acoustic phenomena, the ear verifies perceived differences when they become clearly distinguishable, that is, when the waves tend to reach their maximum amplitudes (volumes). It is interesting that for station KAPA, the calculated time delays are in agreement for the optical and acoustic approach, while the numerical result deviates significantly. This could be an implication for special conditions in the propagation path (e.g. different velocity model, high amplification etc.) that the numerical equations used do not include in the computation process.

## V. Conclusions

The exploration of seismic phenomena through sound offers an insightful way of comprehending their nature, regardless of its value for scientific research. The seismic sound files that were extracted represented these phenomena in an unusual and highly descriptive way, a fact in which the potential of the auditory study of earthquakes partly possibly lies. This potential indeed exists, as is shown by the findings of this study and through the sound data analysis, a better understanding about the extraction and processing of these data was gained.

More specifically, in the case of seismic Doppler study, the data conversion method used proved to be very helpful for the audification of the phenomenon and since the form of data is simple, the interpretation of the results was facilitated. The changes in pitch and duration of the azimuthal distribution of the STFs pointed out the directivity effects clearly and were in accordance with the previous findings about the 7/9/1999 Athens earthquake. Nevertheless, as mentioned before, the normalization by the maximum amplitude value of all the files in the case of the STFs didn't aid the seismic Doppler study significantly because only the compressed and amplified STFs in the direction of the rupture were clearly listenable.

On the contrary, for the study of anelastic attenuation, this normalization proved useful because it sonified the intensity of the attenuation the seismic waves underwent. Combined with the evident differences in the acoustic perception of the S and P wave arrival times at different locations in the Hellenic Arc, it provided an apparent representation of the anelastic attenuation phenomena. As for the calculated S wave arrival time delays, the conclusion is that calculations become more accurate when the computation methods are combined.

Since all methods have their advantages and disadvantages, it is better to verify the results of one method with the others or even resort to more than one methods simultaneously (e.g. optically search a waveform for arrival times while listening to the respective audified file). Both optical and acoustic calculations are definitely less accurate for the attenuated data due to wave arrival time dimming, but it is the same for mathematical calculations in this case.

In summary, it is obvious that auditory seismology cannot yet be dealt as an independent scientific branch, as it is still in an embryonic stage and there is much work to be done for its development. However, its potential is evident and perhaps the most important conclusion in the present state is that it can be addressed individually when one desires to catch the first impression of

audified phenomena and combined with optical and/or mathematical/numerical methods when multidimensional study and verification of results regarding a seismic event is demanded.

## VI. References

- 1) Z. Roumelioti, D. Dreger, A. Kiratzi, and N. Theodoulidis (2003). Slip Distribution of the 7 September 1999 Athens Earthquake Inferred from an Empirical Green's Function Study
- 2) A. A. Skarlatoudis, C. B. Papazachos, B. N. Margaris, C. Ventouzi, I. Kalogeras and the EGELADOS Group (2013). Ground-Motion Prediction Equations of Intermediate-Depth Earthquakes in the Hellenic Arc, Southern Aegean Subduction Area
- 3) David Eberhard (2006). Using Audification to Distinguish Foreshocks and Aftershocks
- 4) Ryan McGee (2009). Auditory Displays and Sonification: Introduction and Overview
- 5) C. P. Snow (1959). The Rede Lecture – Two Cultures
- 6) Florian Dombois (2002). Auditory Seismology: On Free Oscillations, Focal Mechanisms, Explosions and Synthetic Seismograms
- 7) Florian Dombois (2001). Using Audification in Planetary Seismology
- 8) Florian Dombois, Oliver Brodewolf, Oliver Friedli, Iris Rennert, Thomas Koenig† (2008). SONIFYER: A Concept, a Software, a Platform
- 9) Chris Hayward (1992). Listening to the Earth Sing
- 10) Manuela Meier, Anna Saranti (2008). Sonic Explorations With Earthquake Data
- 11) Debi Kilb, Zhigang Peng, David Simpson, Andrew Michael, Meghan Fisher, and Daniel Rohrlick (2012). Listen, Watch, Learn: SeisSound Video Products
- 12) Andrew J. Michael (2011). Earthquake Sounds
- 13) Zhigang Peng, Chastity Aiken, Debi Kilb, David R. Shelly and Bogdan Enescu (2012). Listening to the 2011 Magnitude 9.0 Tohoku-Oki, Japan, Earthquake
- 14) Ingrid Hunstad, Antonella Marsili, Paolo Casale, Massimiliano Vallocchia, and Pierfrancesco Burrato (2013). Seismic Waves and Sound Waves: From Earthquakes to Music
- 15) B. Papazachos (1996). Introduction to Applied Geophysics
- 16) B. Papazachos, C. Papazachou (2003). The Earthquakes of Greece

## Image sources

- 1) Z. Roumelioti, D. Dreger, A. Kiratzi, and N. Theodoulidis (2003). Slip Distribution of the 7 September 1999 Athens Earthquake Inferred from an Empirical Green's Function Study

- 2) A. A. Skarlatoudis, C. B. Papazachos, B. N. Margaris, C. Ventouzi, I. Kalogeras and the EGELADOS Group (2013). Ground-Motion Prediction Equations of Intermediate-Depth Earthquakes in the Hellenic Arc, Southern Aegean Subduction Area
- 3) <http://papernathan.com/?tag=logo>
- 4) <http://csegrecorder.com/interviews/view/interview-with-carl-reine>
- 5) <http://user.physics.unc.edu/~rowan/p24site/p24units/unit14/WCHAP14-6.html>
- 6) <http://russjamieson.com/2014/04/the-voyager-program/>
- 7) <http://seismo.snu.ac.kr/research/directivity.html>
- 8) <http://www.american-buddha.com/cult.pythagsourcebook.fig.htm>
- 9) [http://resource.isvr.soton.ac.uk/spcg/tutorial/tutorial/Tutorial\\_files/Web-basics-pointsources.htm](http://resource.isvr.soton.ac.uk/spcg/tutorial/tutorial/Tutorial_files/Web-basics-pointsources.htm)
- 10) <http://www.wikipedia.org/>

## VII. Appendix

### Matlab script 1 – Source Time Functions (STF) conversions

```
clc
clear
folder=input('Type the folder and file names:', 's');
d=dir(folder); % <- retrieve all names: file(s) and
folder(s)
d1={d.name}.'; % <- file name(s)
nf=numel(d);
unimax=0;
for i=1:nf
    y1=textread(char(d1(i)));
    unimax=max(unimax,max(abs(y1)));
end
for i=1:nf
    y1=textread(char(d1(i)));
    num=length(y1);
    z=zeros(2*num,1);
    z(1:num)=y1;
    for l=num+1:2*num
        z(l)=(-1)*z(2*num+1-l);
    end
    num=2*num;
    unimaxlocal=max(max(abs(z)));
    clear y
    for k=0:99
        y(k*num+1:(k+1)*num,1)=z(1:num);
    end
    y_scale=y/unimax;
    d3=strcat(char(d1(i)), '.wav');
    wavwrite(y_scale,8000,32,d3)
    y_scale1=y/unimaxlocal;
    d4=strcat(char(d1(i)), '_local.wav');
    wavwrite(y_scale1,8000,32,d4)
end
```

## Matlab script 2 – Seismic recording conversion

```
clc
clear
folder=input('Type the folder and file names:', 's');
d=dir(folder); % <- retrieve all names: file(s) and
folder(s)
d1={d.name}.'; % <- file name(s)
nf=numel(d);
h=120.66;
R(1)=148.1215;
R(2)=211.4310;
R(3)=170.9971;
R(4)=121.8140;
R(5)=162.1320;
R(6)=213.6115;
unimax=0;
for i=1:nf
    y1=textread(char(d1(i)));
    ycor=(R(i)/h)^1.7;
    ydb=10*log10(ycor);
    y1=y1*ycor;
    unimax=max(unimax,max(abs(y1)));
end
for i=1:nf
    clear y1;
    d1(i);
    y1=textread(char(d1(i)));
    ycor=(R(i)/h)^1.7;
    ydb=10*log10(ycor);
    y1=y1*ycor;
    maxlocal=max(abs(y1));
    y_scale=y1/unimax;
    d3=strcat(char(d1(i)), '.wav');
    wavwrite(y_scale,2500,32,d3)
    y_scale1=y1/maxlocal;
    d4=strcat(char(d1(i)), '_local.wav');
    wavwrite(y_scale1,2500,32,d4)
end
```

### Matlab script 3 – Hypocentral distance and S - P arrival time delay calculations

```
clc
clear
h=120.66;
fE=36.6110;
lE=26.8660;
fS=[36.9150,36.6216,36.7449,36.0119,35.5472,35.1147];
lS=[25.9788,24.9197,26.9517,27.8197,27.1612,26.2170];
for i=1:6
[dist,az] = distance(fE,lE,fS(i),lS(i));
D=(40009.88/360)*dist;
r=sqrt(D*D+h*h)
Tp=(r/7.63)*0.04;,%disp('sec')%----->sample rate = 2500
sps
Ts=(r/4.27)*0.04;,%disp('sec')%-----> sample rate = 2500
sps
dt=Ts-Tp,disp('sec')
end
```

## CD track listing

1. Athens Doppler local – L
2. Athens Doppler local – S
3. Athens Doppler uni – L
4. Athens Doppler uni – S
5. FOLE
6. FOLE local
7. AMOS
8. AMOS local
9. KOSI
10. KOSI local
11. ZKR
12. ZKR local
13. KAPA
14. KAPA local
15. RHOS
16. RHOS local
17. \* FOLE local with FFT
18. \* AMOS local with FFT
19. \* KOSI local with FFT
20. \* ZKR local with FFT
21. \* KAPA local with FFT
22. \* RHOS local with FFT

\*Video